AD-A064 745 CATHOLIC UNIV OF AMERICA WASHINGTON D C SCHOOL OF EN--ETC F/G 8/10
THE ROLE OF MICRO WATER DROPLETS ON THE TRANSPORT OF HEAT AND M--ETC(U)
1978 S C LING, T W KAO, A I SAAD N00014-77-C-0017

UNCLASSIFIED NL

END
DATE FILMED
4 -79
DDC

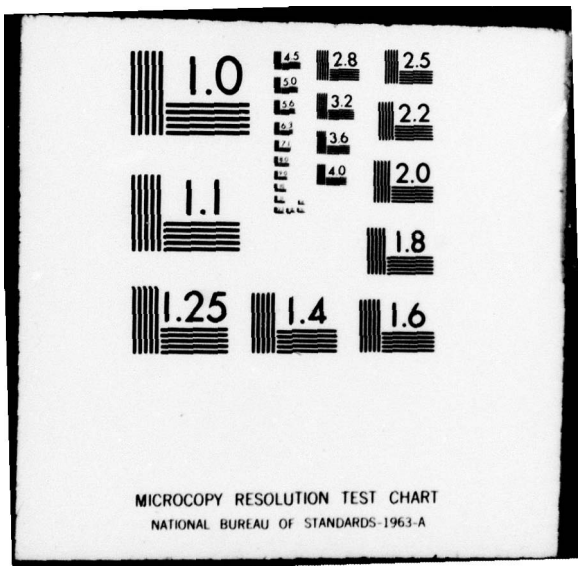
1.0
1.1
1.25
1.4
1.6
1.8
2.0
2.2
2.5
2.8
3.2
3.6
4.0
4.5
5.0
5.6
6.3
MICROCOPY RESOLUTION TEST CHART
NATIONAL BUREAU OF STANDARDS-1963-A

(12) SC

(6) THE ROLE OF MICRO WATER DROPLETS ON THE TRANSPORT OF HEAT AND MOISTURE FROM THE OCEAN AND LAKE

(10) by S. C. Ling, T. W. Kao, and A. I. Saad

The Catholic University of America
School of Engineering
Washington, D.C. 20064

(11) 1978

(12) 17p.

INTRODUCTION

The ever increasing demand for new water resources and better long range weather forecasting requires a fundamental understanding of the complex mechanics of sea-air interaction, because it controls the main source of moisture and energy in the atmosphere. This paper represents a progress report on one aspect of the study - in particular the role of micro water droplets. In the past, the fields of heat and moisture were treated as independent systems indirectly related to the momentum field through the eddy diffusivity. This resulted in the need for an artificial increase in the eddy diffusivities for both the humidity and temperature fields in order for the analyses to fit the experimental data, see reviews by Roll (6), Panofsky (5), and Monin and Yaglom (4). Recently it was shown by Ling and Kao (2) that these fields are strongly coupled through the water droplets produced by sea sprays and whitecaps; i.e., the micro water droplets contribute to an important source of moisture to the humidity field while the latent heat of evaporation provides a strong heat sink for the temperature field. The resultant stratification of the temperature field further influences the stability of the momentum field, which in turn affects the whole exchange process. Following this preliminary work was an improved theory which took into account the size distribution

(15) Contract N00014-77-C-0317

of droplets and their free fall velocities. This work (3) was published in the Proceedings of the NATO Symposium on Turbulent Fluxes through the Sea Surface, Wave Dynamics and Prediction, France, 1977. In this paper we shall describe some further improvements to the theory by taking into account the limited data obtained from the 1977 (Joint Sea Air Interaction Project) JASIN experiment. All results presented in this paper should be considered as preliminary, since we are still in the process of improving the analytical model through more detailed laboratory simulations and field measurements. Presently the analytical model is sufficiently realistic to indicate which droplet sizes are important to the evaporation process under a given atmospheric condition. This and other new improvements to the theory will be discussed in the following sections.

GOVERNING EQUATIONS

The basic governing equations for the fields of heat, humidity, water droplets and momentum were derived from the general transport equation (2). Because of the large horizontal extent of the ocean compared with the thickness of the atmospheric surface layer, it is possible to treat this layer as being quasi steady and uniform in the horizontal direction. In the following, we shall only give detailed explanation to the new and improved parts of the equations and refer the rest to the cited references.

The normalized equation for the water droplets can be expressed as

$$\bar{K}\frac{\partial^2 \bar{Q}_n}{\partial \bar{z}^2} + \frac{\partial \bar{K}}{\partial \bar{z}}\frac{\partial \bar{Q}_n}{\partial \bar{z}} + \bar{S}_{Qn} - \bar{W}_n \frac{\partial \bar{Q}_n}{\partial \bar{z}} + 12\frac{\rho_a}{\rho_w} D_v \left(\frac{\epsilon}{U_{10}^2}\right) U_{10}\, H_s(T)(1-H_o^s)(1-\bar{H})$$

$$\times \left[\frac{(1+0.25R_{n+1}^{0.5})d_{n+1}\bar{Q}_{n+1}}{d_{n+1}^3 - d_n^3} - \frac{(1+0.25R_n^{0.5})d_n \bar{Q}_n}{d_n^3 - d_{n-1}^3}\right] = 0. \qquad (1)$$

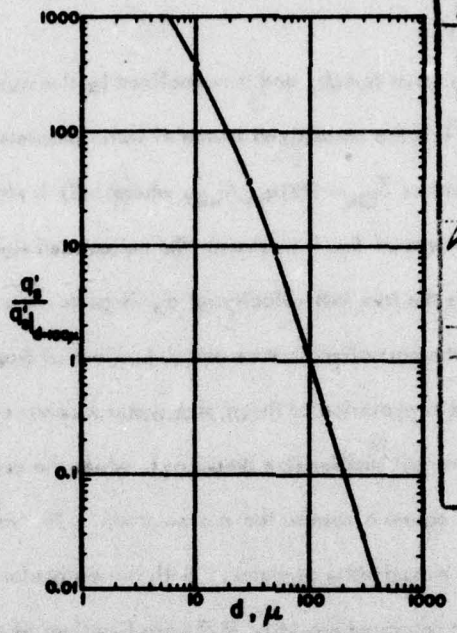

Fig. 1. Normalized water droplet production rate for different sizes of droplets. Data was taken over hydraulic jumps with wide range of energy levels, from Ling, Saad and Kao, Proc. of the 1977 NATO Symposium cited in text.

The water droplets are treated as discrete droplet size groups denoted by subscript n. The first two terms of Eq. 1 represent the rate of change in the normalized droplet concentration $\bar{Q}_n$ due to eddy diffusivity K, where K is normalized by the mean wave height ϵ and the 10m wind U_{10} as $\bar{K} = K/\epsilon U_{10}$. The normalized droplet concentration is defined as $\bar{Q}_n = Q_n U_{10}/q_{s2}$, where Q_n is the droplet concentration for size group n and q_{s2} is the mean surface flux of size group 2. Because the distribution of the surface flux ratio $q_s'/q_s'|_{d=100\mu}$ for different droplet size d was found to be universal for all intensities of wave breaking, see Fig. 1, it is convenient to select an important size group as the reference, and referring the fluxes for the other size groups as fixed ratios of the reference group. The vertical coordinate z is

defined from the mean wave trough, and is normalized by the wave height ϵ as $\bar{z}$. The third term of Eq. 1 is the normalized source of water droplets produced by whitecaps and sea sprays expressed as $\bar{S}_{Qn} = S(\bar{z}) q_{sn}/q_{s2}$, where $S(\bar{z})$ is the source distribution factor (2). The fourth term of Eq. 1 represents the normalized sink due to free fall of droplets, where $\bar{W}_n$ is the free fall velocity of d_n droplets normalized by U_{10}. The fifth term of Eq. 1 is the normalized source and sink effect of droplets due to evaporation; i.e., the evaporation of the n size group droplets causes a loss of droplets to be transferred to the next smaller size group $n-1$, while the evaporation of the next larger size group $n+1$ causes a gain to the n size group. The variable ρ_a is mass density of air and ρ_w mass density of water. Both the molecular diffusivity of water $D_v(T)$ and the specific saturated humidity $H_s(T)$ are functions of the absolute air temperature T. The variable H^* is the relative humidity, H_o^* the relative humidity at the reference height $\bar{z}_o$, $\bar{H}$ the normalized humidity defined as $(H_o^* - H^*)/(H_o^* - 1)$, and R_n the Reynolds number based on the terminal fall velocity W_n and droplet size d_n.

The normalized equation for the humidity field can be expressed as

$$\bar{K}\frac{\partial^2 \bar{H}}{\partial \bar{z}^2} + \frac{\partial \bar{K}}{\partial \bar{z}}\frac{\partial \bar{H}}{\partial \bar{z}} + \sum_{n=1}^{m} 2(1+0.25R_n^{0.5})\pi D_v \left(\frac{q_{s2}}{U_{10}^2}\right)\left(\frac{\epsilon}{U_{10}^2}\right) U_{10}^2 d_n \times H_s(T)(1-H_o^*)(1-\bar{H})\bar{Q}_n = 0 . \qquad (2)$$

The first two terms of Eq. 2 represent the rate of change in $\bar{H}$ due to eddy diffusivity $\bar{K}$, and the third term represents the source of humidity due to the evaporation of water droplets. Since the production of droplet flux is expected to be proportional to U_{10}^2, the parameter (q_{s2}/U_{10}^2) is one of the most important constants to be determined

in this work. Similarly the mean wave height ϵ is known to be proportional to U_{10}^2, therefore (ϵ/U_{10}^2) can generally be taken to be 0.00029 sec^2/cm.

The normalized temperature field can be expressed as

$$\bar{K}\frac{\partial^2\bar{T}}{\partial\bar{z}^2} + \frac{\partial\bar{K}}{\partial\bar{z}}\left(\frac{\partial\bar{T}}{\partial\bar{z}} - \bar{\Gamma}\right) - \sum_{n=1}^{m}\frac{L_h}{C_p|T_w - T_o|}2(1+0.25R_n^{0.5})\pi D_v\left(\frac{q_s 2}{U_{10}^2}\right)\left(\frac{\epsilon}{U_{10}^2}\right)U_{10}^2 d_n$$

$$\times H_s(T)(1-H_o^*)(1-\bar{H})\bar{Q}_n = 0 . \qquad (3)$$

The normalized temperature is defined as $\bar{T} = (T - T_o)/|T_w - T_o|$, where T is the absolute air temperature, T_w the reference absolute sea surface temperature, and T_o the absolute reference air temperature at the reference height $\bar{z}_o$. The normalized adiabatic lapse rate of the atmosphere is defined as $\bar{\Gamma} = \Gamma\epsilon/|T_w - T_o|$, where the adiabatic lapse rate Γ is generally taken to be $-0.0001\ ^\circ C/cm$. The third term of Eq. 3 represents the latent heat sink for the temperature field due to the evaporation of water droplets. The variables $L_h(T)$ and C_p are the coefficients of latent heat of evaporation for water and specific heat for air, respectively.

Finally the momentum equation for wind can be expressed as

$$\rho_a\frac{\partial}{\partial z}K(z)\frac{\partial U}{\partial z} - \frac{\partial p}{\partial x} - C_d A(z)\frac{\rho_a(U-U_c)^2}{2} = 0 . \qquad (4)$$

The first term of Eq. 4 is the rate of change in momentum due to eddy diffusivity $K(z)$. The second term represents the pressure gradient force per unit volume in the mean wind direction x. Because the atmospheric surface layer is generally within 100m thick, the effect of $\partial p/\partial x$ can no longer be neglected at $z > 15m$. We shall attempt to relate this term to the sea surface shear stress τ_o or the friction coefficient C_f as $\tau_o = C_f \rho_a U_{10}^2 \simeq - z_m \partial p/\partial x$, where z_m is the nominal height from which the geostrophic

pressure gradient $\partial p/\partial x$ is physically integrated downward to maintain τ_o. The third term of Eq. 4 represents the drag force offered by the moving waves on a unit horizontal strip of air volume. The function A(z) is the total effective drag areas offered by the parts of waves which are within the unit volume. That is, we treat waves as moving drag centers within an air space. The drag coefficient C_d is generally taken to be unity. The local mean velocity of wind U minus the phase velocity of waves U_c in the direction of the wind gives the effective wind acting on the waves. The normalized momentum equation may now be expressed as

$$\bar{K}\frac{\partial^2 \bar{U}}{\partial z^2} + \frac{\partial \bar{K}}{\partial z}\frac{\partial \bar{U}}{\partial z} + \frac{C_f}{\bar{z}_m} - 0.5A(z)(\bar{U}-\bar{U}_c)^2 = 0 , \qquad (5)$$

where $\bar{U} = U/U_{10}$, $\bar{U}_c = U_c/U_{10}$, and $\bar{z}_m = z_m/\epsilon$. Under strong wind condition, $\bar{z}_m$ may be estimated from a geostrophic pressure gradient of 10mb/250km to give a value of approximately 23. Hence, for general use, the term $C_f/\bar{z}_m$ may be taken to be a constant equal to 0.0001. At low levels this term is negligible compared with the other terms. The fourth term of Eq. 5 only has values below the wave crest. We believe that the present treatment for the atmospheric surface boundary layer is more physically meaningful and applicable than the usual empirical log-linear profile approximation which requires an artificial displacement height and neglects the pressure gradient. Because the momentum equation is only coupled with the other transport equations through K, it can be used to check the validity of K used in the calculation; i.e., by comparing the analytical wind profiles with the experimental data taken under a known atmospheric condition.

METHOD OF SOLUTION

It has been argued before that the eddy diffusivity K should be universally applicable to all transportable quantities, because the molecular diffusivity of these quantities are all negligibly small with respect to K. In the analytical model we consider that K can be modified by the stability of the air system and is expressible as functions of the Monin-Oboukhov length parameter, see Panofsky (5) and Ling and Kao (2). After reviewing many actual wind profiles taken under neutral condition and using Eq. 5, we have found that the normalized eddy diffusivity $\bar{K}_u$ under neutral condition should be modified from the one first proposed in reference (2) to a new form as shown by the dashed curve in Fig. 2a. The value for $\bar{K}_u$ above $\bar{z}=5.5$ should be increased to a constant value of 0.125. At lower levels, it should still increase linearly with height as $0.02\bar{z}$ up to $\bar{z}=5.0$ instead of 2.5. In performing the numerical calculation a trial distribution of $\bar{K}(\bar{z})$ was first estimated through $\bar{K}_u$ and the Monin-Oboukhov stability length parameter based on a Bowen ratio of $0.07(T_w - T_o)$, see Ling and Kao (2). It was then successively refined with the Bowen ratio based on more accurate vertical fluxes of heat and moisture derived from the calculated solutions.

Before the coupled set of equations can be solved, one must define both the droplet size distribution and the flux parameter q_{s2}/U_{10}^2. For the following examples we chose to represent the droplet size distribution in n=5 groups with d_n = 10, 40, 80, 140, and 300 μ, and the corresponding droplet bandwidths Δd_n = 20, 40, 40, 80, and 240 μ, respectively. Thus from the normalized droplet production curve, Fig. 1, one can find the ratio of production rates for different groups of droplets as

$$\frac{q_{sn}}{q_{s2}} = \frac{\Delta d_n \, q'_{sn}}{\Delta d_2 \, q'_{s2}} = 12,\ 1,\ 0.1,\ 0.03,\ \text{and}\ 0.009,\ \text{respectively; where}\ q'_{sn}\ \text{is}$$

the surface droplet flux for a droplet size d_n. Presently there is no known technique to obtain the droplet flux parameter q_{s2}/U_{10}^2 directly from the ocean. It may be deduced indirectly from the measured droplet concentration or the concentration of salt nuclei in the upper atmosphere (6, p.62). From our present theory we have found that this parameter has a strong effect on the temperature field as well as the droplet concentration field. Thus by checking the analytical solutions obtained with different q_{s2}/U_{10}^2 values against a corresponding set of field data, one may ultimately determine the best value to use. We have tentatively found that $q_{s2}/U_{10}^2 = 0.00012$ drops sec/cm^4 gives very reasonable results. It will be used for all examples presented in this paper. Thus before this parameter can be defined accurately, all solutions derived from it must only be considered as preliminary examples.

With both $\bar{K}_u$ and q_{s2}/U_{10}^2 tentatively quantified, one may proceed to solve the coupled set of transport equations with suitable boundary values and conditions. A unique solution can be found for any set of boundary values of T_o, H_o^*, T_w, and U_{10}. For the examples given in the following section, a constant reference height of $z_o = 20$ was used since our present interest is limited to the atmospheric surface layer. When the model for this layer is fully developed it can be readily merged with the upper atmospheric as well as the oceanic surface layers for a more complete system simulation. Because the numerical techniques used to solve the problems were quite standard and had been described in the cited references, they need not be restated.

From the calculated solutions, the vertical fluxes may be accurately determined at any given z levels. The sensible heat flux can be expressed as

$$q_h|_z = -\rho_a C_p U_{10} |T_w - T_o| \bar{K}|_z \left(\frac{\partial \bar{T}}{\partial z}\Big|_z - \bar{\Gamma} \right), \qquad (6)$$

and the water mass flux can be expressed as

$$q_w|_{\bar{z}} = \frac{\pi}{6}\rho_w\left(\frac{q_{s2}}{U_{10}^2}\right)U_{10}^2\sum_{n=1}^{m} d_n^3\left(-\bar{K}|_{\bar{z}}\frac{\partial\bar{Q}_n}{\partial\bar{z}}\Big|_{\bar{z}} - \bar{W}_n\bar{Q}_n|_{\bar{z}}\right) - \rho_a U_{10}(1-H_o^*)H_s(T)\bar{K}|_{\bar{z}}\frac{\partial\bar{H}}{\partial\bar{z}}\Big|_{\bar{z}} . \quad (7)$$

It should be noted that the present model contains various sources and sinks in the field equations, therefore the vertical fluxes are no longer constant.

RESULT AND CONCLUSION

With the improved analytical model we may now compare the result with the actual field data in a more realistic manner. Unfortunately, complete set of wind, temperature, humidity, and droplet concentration profiles are still not available at this moment, but we hope to obtain them during the 1978 JASIN experiment over the North Atlantic Ocean. Meanwhile, we may make some preliminary comparison with a few good but incomplete field soundings. The following examples were classified in terms of whether the sea was warmer or cooler than the upper air mass. To obtain the true differential temperature between the upper air mass at the 200-400m level and the sea one must extrapolate the upper air temperature downward along the dry adiabat to the sea surface and compare this potential temperature T_p with respect to the sea surface temperature T_w, see Fig. 2b.

In general air is cooler than the ocean. When a mass of air has traversed a long distance over a warm sea, its temperature should not be too different from that of the water. This is represented by case 1 shown in Fig. 2b. It is a sounding taken by Emmons (1, p.27). We note that the ocean was warmer than the upper air by $T_w - T_p = 1.8^{\circ}C$, and the air was homogeneous upward to 300m with the air temperature decreasing at the adiabatic lapse rate. A simulation of this case up to a reference

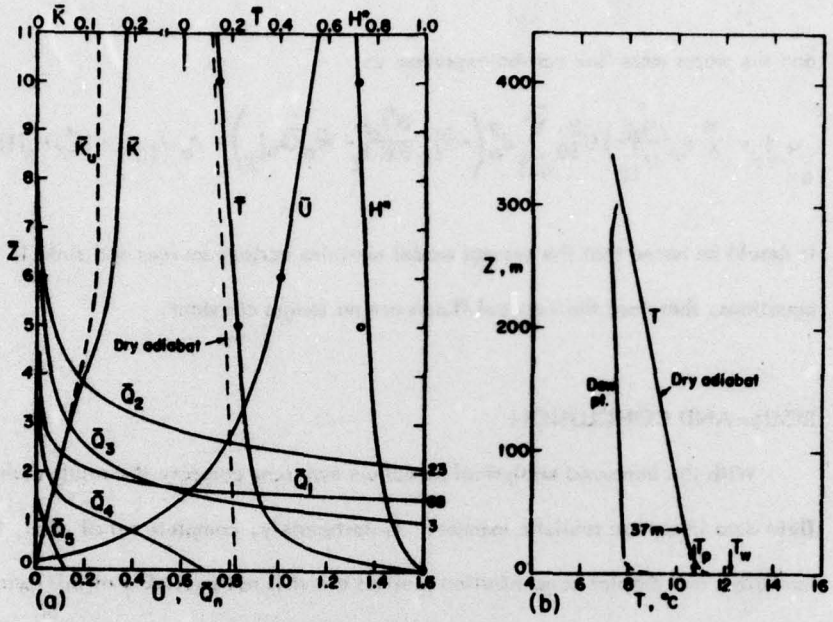

Fig. 2. a) Simulation of warm sea, Case 1. b) Sounding by Emmons (1, p. 27).

height of $z_o = 37$ m, with $T_o = 10.4^\circ$C, $H_o^* = 0.65$, $T_w = 12.2^\circ$C, and $U_{10} = 8$ m/sec is shown in Fig. 2a. Only the lower half of the calculated data was plotted. Note that the adiabatic lapse rate was almost reached at $\bar{z} > 10$. Both the temperature and humidity profiles closely simulated the field soundings. That is, at $\bar{z} > 10$ there was almost no potential temperature gradient or no sensible heat flux. The sensible heat from the ocean was mostly absorbed by the latent heat of water droplets. Indeed this is the most prevalent feature found in all warm oceans. The net water mass flux was found to be $q_w = 1.3 \times 10^{-5}$ g/cm^2 sec, which gave a net heat flux from the sea of 7.6×10^{-3} cal/cm^2 sec. These large fluxes greatly destabilized the air system causing uniform mixing of air up to a great height of over 300 m where the humid air was

condensed into heavy cloud. Thus the important latent heat transfer cycle is clearly evident. The calculated $\bar{K}$, $\bar{U}$, and $\bar{Q}_n$ are also shown in the figure. There was no field data for $\bar{Q}_n$, however we note that the calculated concentration of droplets was highly stratified with very little remaining above $\bar{z}=3$. The values of $\bar{Q}_1$, $\bar{Q}_2$, and $\bar{Q}_3$ at the wave trough were beyond the plotting range of the graph, but their values were indicated on the left border of the figure. One notes that the concentration for the 10μ size droplets $\bar{Q}_1$ above $\bar{z}=1.5$ was less than the larger 40μ droplets $\bar{Q}_2$ due to faster evaporative loss of the submicro droplets. On the other hand, the concentration for the 300μ droplets $\bar{Q}_5$ were quickly depleted by their fast free fall velocity.

Case 2 represents a cooler sea with almost no sea to air temperature difference, $T_w - T_p = -0.2^{\circ}C$, see Fig. 3b. This sounding was also taken by Emmons (1, p. 21).

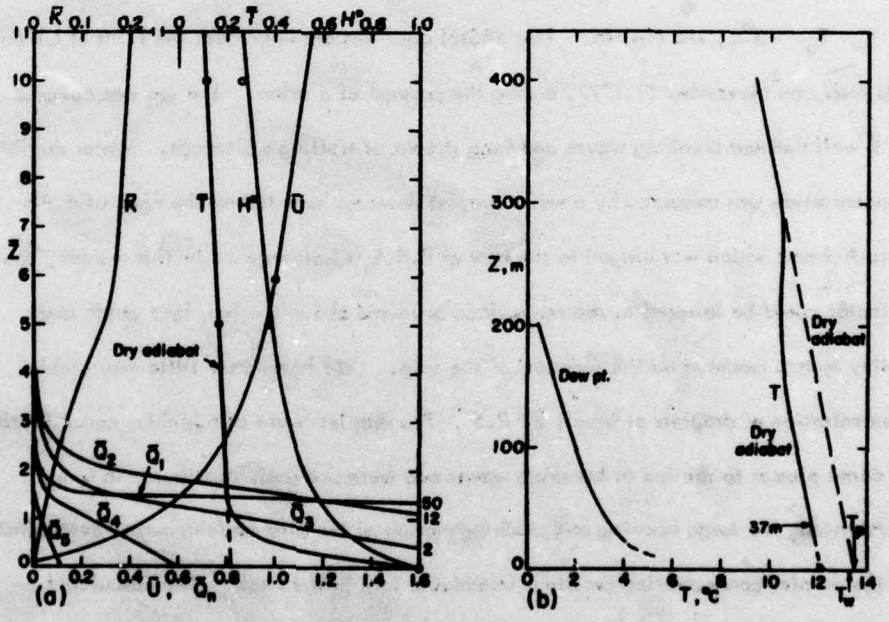

Fig. 3. a) Simulation of cooler sea, Case 2. b) Sounding by Emmons (1, p. 21).

There was a cooler and more humid surface layer of air below a warmer and very dry upper air. Thus both the sea and the upper air were heating the surface layer of air. The physical existence of this more humid and cooler layer of air could only be attributed to the moisture production and the latent heat absorption by the water droplets. The lower 37m of this layer of air was simulated by the present theory and was shown in Fig. 3a, with $T_o = 11.7^oC$, $H_o^* = 0.12$, $T_w = 13.3^oC$, and $U_{10} = 8 m/sec$. The air temperature quickly reached the adiabatic lapse rate at $\bar{z} > 1.5$, indicating that this surface layer was highly unstable and well mixed to a height of 200m where it merged into the upper air mass. The physical reason for the lack of any sensible heat flux above the waves was the same as the warm sea case. Due to low atmospheric humidity, the height of droplet concentration was greatly reduced; i.e., nearly all droplets had evaporated at $\bar{z} > 2$.

Case 3 represents a more cooler sea with a sea to upper air temperature difference of $T_w - T_p = -3^oC$, see Fig. 4b. This JASIN data was obtained over the Firth of Clyde, Scotland, on November 5, 1977, during the passage of a storm. The sea was covered with well defined breaking waves and long streaks of trailing whitecaps. Water droplets concentration was measured by a water droplet detector mounted on the apex of a 9m long A-frame which was hinged to the bow of R.R.S. Challenger. In this manner, the detector could be lowered to the sea surface or raised above the bow by a cable and pulley system mounted on the foremast of the ship. We found very little measurable concentration of droplets at levels $\bar{z} > 2.5$. The droplets were also highly concentrated in dense plumes to the lee of breaking waves and were unevenly distributed in space. In addition, the large heaving and pitching motion of the ship made accurate determination of the droplet concentration profile a formidable task in the field. The calculated

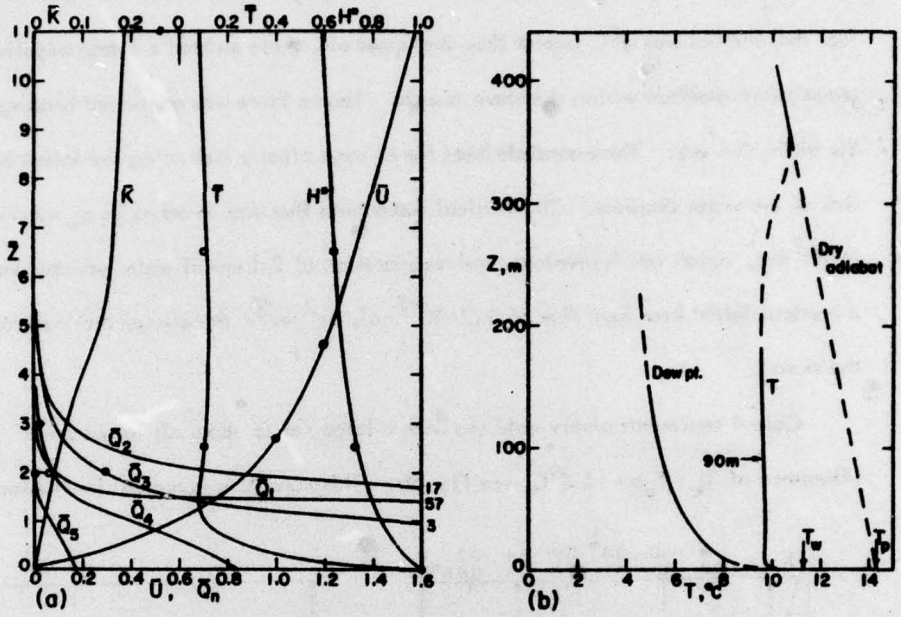

Fig. 4. a) Simulation of cold sea, Case 3. b) Sounding taken during passage of a storm, 1977 JASIN experiment.

droplet concentration profiles gave a generally strong, low level, stratification of droplets as was observed in the field. Due to evaporation, the concentration of the 10μ droplets $\bar{Q}_1$ at $\bar{z} > 1.5$ was less than the 40μ droplets $\bar{Q}_2$. This result was contrary to the field data which indicated much larger $\bar{Q}_1$. It was possible that the field data had included the counting of salt nuclei as submicro droplets. In general, the measured droplet concentrations for the larger droplet groups were less than the predicted values. This problem will have to be resolved by additional future studies. The atmospheric simulation for this case was made below a reference height of $z_o = 90$m, with $T_o = 9.6^\circ$C, $H_o^* = 0.5$, $T_w = 11.3^\circ$C, and $U_{10} = 12.5$m/sec. In Fig. 4a, we note that the temperature profile above the wave crest was almost vertical. It indicated

a positive potential temperature gradient or heating by the upper air. In spite of the fact that the sea was 3°C cooler than the upper air, there existed a strong negative temperature gradient within the wave trough. Hence there was continued heating of the air by the sea. These sensible heat fluxes were clearly balancing the latent heat sink of the water droplets. The vertical water mass flux was found to be $q_w = 2.9 \times 10^{-5}$ g/cm^2 sec, which was equivalent to an evaporation of 2.5 cm of water per day and a vertical latent heat heat flux of 1.7×10^{-2} cal/cm^2 sec - the energy that was fueling the storm.

Case 4 represents a very cold sea with a large sea to upper air temperature difference of $T_w - T_p = -11.8$°C, see Fig. 5b. This condition is typical for the formation

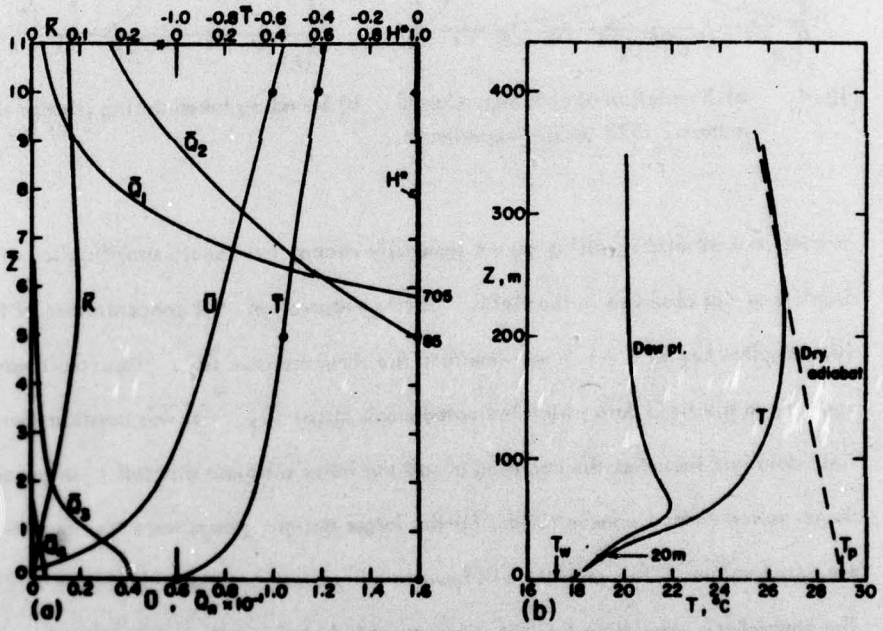

Fig. 5. a) Simulation of very cold sea with light fog, Case 4. b) Sounding by Emmons (1, p. 57).

of a strong inversion and creation of a very humid surface layer which can easily developed into dense sea fog. This sounding was taken by Emmons (1, p. 57) over the Atlantic Ocean at 40°N and 71°W, with light sea fog below the 20m level and warm dry air above 200m. The analytical simulation was for a reference height of z_o=20m, with T_o=19.2°C, H_o^*=0.98, T_w=17.2°C and U_{10}=6m/sec. One notes in Fig. 5a that only under very cold sea will the air heat the sea as indicated by the positive temperature gradient at sea level. Above z=20m, see Fig. 5b, there was a general increase in the temperature gradient. This increase was due to the evaporation of droplets at higher elevations, thus causing a strong inversion layer which tended to cap off the humid surface layer. Due to the large increase in the droplet concentration, the plotted scale for $\bar{Q}_n$ was increased by 10. Note that only the d_1 and d_2 size droplets were able to reach high elevation to form sea fog. Here again at $\bar{z}>6$ the value of $\bar{Q}_2$ was greater than $\bar{Q}_1$. However, the actual concentration of the d_1 droplets at sea level was 6 drops/cm^3 which is enough for creating a light fog. The sensible heat flux at $\bar{z}$=2 was -7.8×10^{-4} cal/cm^{2}sec and the mass water flux was 1.1×10^{-6} g/cm^{2}sec. The water flux was small compared with the other cases, because there was essentially no evaporation from the sea surface or from large water droplets due to high humidity at sea level. The water flux was mainly contributed by the evaporation of the d_1 and d_2 droplets at high elevation. To make this clear, we have shown in Fig. 6 the normalized water mass flux contributed by different size groups of droplets at the $\bar{z}$=2 level. It is expressed as $q_{dn}/q_d\Delta d_n$, where q_{dn} is the vertical mass flux of the d_n size droplets and q_d is the total droplet mass flux. Smooth curves were drawn over the data blocks such that the areas remained unity under the curves. One notes that for case 4 the flux was mainly contributed by the

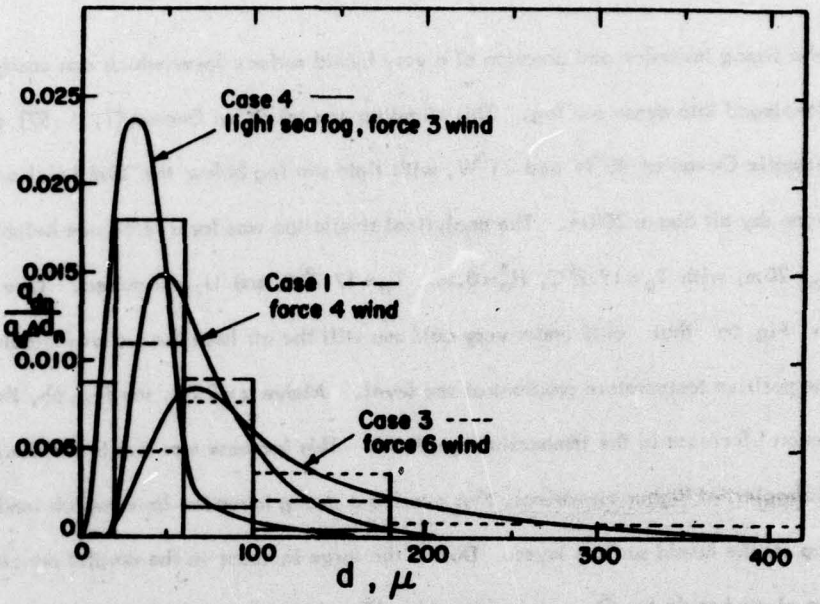

Fig. 6. Contribution to the vertical droplet mass flux at $\bar{z}=2$ by different sizes of water droplets, for cases 1, 3, and 4.

10 to 60μ fog droplets. For case 3, under force 6 wind, the main contribution was broaden to the 30 to 300μ droplets. This was due to a wind force sufficient to keep the large droplets long enough in air for evaporation. Thus under hurricane wind the contribution from the large droplets will become very large. For case 1, with force 4 wind, the main contribution was narrowed down to the 30 to 140μ droplets. There was almost no contribution from the 1 to 20μ droplets, because these droplets had already been evaporated before reaching the $\bar{z}=2$ level.

We may briefly conclude that the present analytical model has clarified many mysteries concerning the complex mechanics of the sea-air interaction. It is hoped that with further refinements to the model an accurate means could be found to estimate under all climatic conditions the various fluxes over large bodies of water.

ACKNOWLEDGMENTS

We wish to thank the JASIN organization in particular R.T. Pollard of the Institute of Oceanographic Sciences, England, and D.E. Ellett of the Scottish Marine Biological Association for their most generous hospitality, technical support, and the use of their research ship R.R.S. Challenger. This work was supported by the Ocean Science and Technology Division of the Office of Naval Research under contract N00014-77-C-0017.

REFERENCES

1. Emmons, G., "Vertical Distributions of Temperature and Humidity over the Ocean between Nantuck and New Jersey", Paper in Physical Oceanography and Meteorology, Vol. 10, No.3, Woods Hole, Massachusetts, 1947.
2. Ling, S. C., and Kao, T. W., "Parameterization of the Moisture and Heat Transfer Process over the Ocean under Whitecap Sea States", J. of Phys. Oceanogr., Vol. 6, No. 3, 1976, pp. 306-315.
3. Ling, S. C., Saad, A., and Kao, T. W., "Mechanics of Multiphase Fluxes over the Ocean", Proc. of NATO Symposium on Turbulent Fluxes through the Sea Surface, Wave Dynamics and Prediction, Plenum Pub., New York, N.Y., 1978, pp. 185-197.
4. Monin, A. S., and Yaglom, A. M., Statistical Fluid Mechanics: Mechanics of Turbulence, Vol. 1, MIT Press, Cambridge, Massachusetts, 1971, pp. 440-442.
5. Panofsky, H. A., "The Atmospheric Boundary Layer below 150meters", Annual Review of Fluid Mechanics, M. VanDyke, ed., Vol. 6, Annual Review Inc., Palo Alto, California, 1974, pp. 147-177.
6. Roll, H. U., Physics of the Marine Atmosphere, 2nd ed., Academic Press, New York, N.Y., 1971.